XXI IMEKO World Congress "Measurement in Research and Industry"
August 30 - September 4, 2015, Prague, Czech Republic

PROGRESS ON MAGNETIC SUSPENSION FOR THE NIST VACUUM-TO-AIR MASS DISSEMINATION SYSTEM

Corey Stambaugh [1,*], *Edward Mulhern* [1], *Eric Benck* [1], *Zeina Kubarych* [1], *and Patrick Abbott* [1]

[1] National Institute of Standards and Technology, Gaithersburg, U.S.A., *corey.stambaugh@nist.gov

Abstract - The redefined kilogram will be realized in vacuum and NIST is developing a magnetic suspension system to disseminate the standard to air. This paper details the progress to characterize and improve the performance of the magnetic suspension portion of the system. Effort has been made to determine the magnetic field within the system through simulation and experiment. To increase stability interferometry is being integrated into the system.

Keywords: mass, balance, magnet, suspension, interferometry

1. INTRODUCTION

In 2018, the SI unit of mass, the kilogram, is expected to be redefined so that its magnitude is set by fixing the value of the Planck constant. The reasons behind this change [1] include the measured difference in mass between the international prototype kilogram and the other official copies produced during the same time period [2]. Despite this redefinition, the general process of mass dissemination will remain largely the same and thus continued use of mass comparators and artifacts is necessary. However, the primary realization of the new kilogram will take place in vacuum, therefore a method of vacuum-to-air transfer is needed.

The common method of vacuum-to-air mass comparison is to use sorption standards to develop empirical models to account for mass changes that air introduces when the test mass is removed from vacuum [3]. At the National Institute of Standards and Technology a different approach is being pursued. Here, the standard artifact, kept in vacuum, is directly compared, using the same high precision balance, to a test mass in air. The mass comparison is carried out by coupling the two systems through a magnetic suspension method [4]. This approach eliminates the need to correct the test mass value to account for environmental sorption effects.

Currently, the magnetic suspension system (MSS) is going through an upgrade as the entire setup is moved into a new laboratory. In this paper we discuss the work being done during this time to characterize and improve the overall performance of the MSS. The MSSs discussed here encompass two systems. The first, which will be referred to as the real MSS, represents the final upgraded system. The second, referred to as the test MSS, is a prototype built for testing improvements to the magnet suspension before integration into the real MSS. In general the magnetic suspension systems can be broken down into several key components: (1) the actuator which consists of the electromagnetic coil and permanent magnets, (2) the sensor which consists of a Hall probe and interferometer, and (3) the feedback electronics and software. Through these studies we aim to improve the system stability and increase the overall precision of the mass comparison measurements.

2. MAGNETIC SUSPENSION SYSTEM

Figure 1 shows a schematic of the magnetic suspension system, while Fig. 2a identifies the components of the magnet assembly used in the real MSS. The entire assembly is housed in the upper and lower chambers of an aluminum vacuum vessel. A precision mass comparator is located in the evacuated upper chamber; its mass pan and the upper magnet assembly are hung from the comparator. The upper magnet assembly consists of a rare-earth cylinder magnet with a soft-iron cylinder placed above it; the iron serves to enhance the field. Wrapped around the permanent magnet is a multi-turn coil. Surrounding the magnet are two layers of mu-metal shielding. This reduces the spatial extent of the magnet's field and limits its interaction with any surrounding magnetic materials. The lower chamber at atmospheric pressure contains a second magnet assembly with a mass plate connected below it. The lower magnet assembly is similar to the upper except there is no coil. Embedded in the flange separating the upper and lower chambers is a Hall sensor. In the upgraded system an optical measurement sensor will be attached directly below the lower magnet assembly.

2.1. Mass Measurement

Using this system, mass comparison could be carried out in the following way. First, a reference mass, calibrated using the Watt balance [5], is placed on the mass pan positioned above the magnet assembly in the upper chamber. The lower magnet assembly, without the test mass, is then suspended and a reading of the mass using the balance is carried out. Next the magnetic suspension is stopped, the reference mass is removed from the upper pan and a test mass is placed on the lower plate, then the lower assembly is re-suspended and a measurement of the test mass is made. The test mass is then determined to be the calibrated mass of the standard plus the difference in the two mass measurements. Additional adjustments are made to account for the buoyancy correction due to air and the gravitational change due to the differing heights of the measured masses.

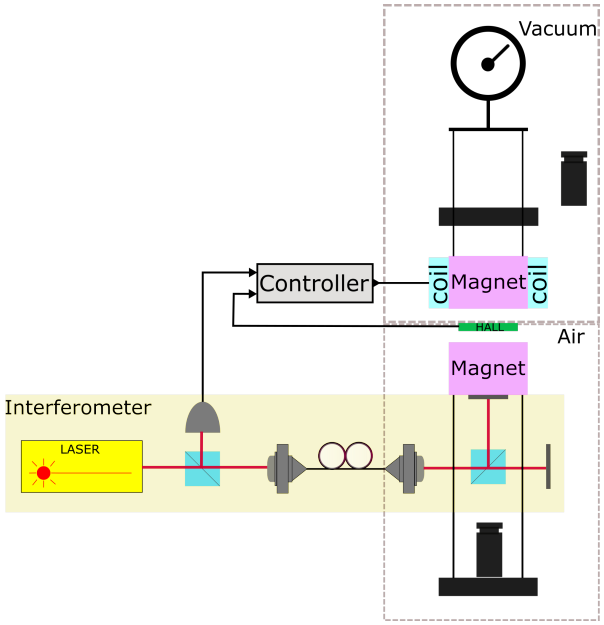

Fig. 1. Schematic of the magnetic suspension system for vacuum-to-air mass comparison. The reference mass is housed in the upper vacuum chamber along with the mass balance. The test mass is placed in the lower chamber. The relative separation of the upper and lower assembly is monitored by a Hall probe. In the new design an interferometric signal will be used for monitoring sub-micron motion. These two signals are fed into the servo controller; the output drives the electromagnetic coil stabilizing the suspended assembly and improving the precision of the mass measurement.

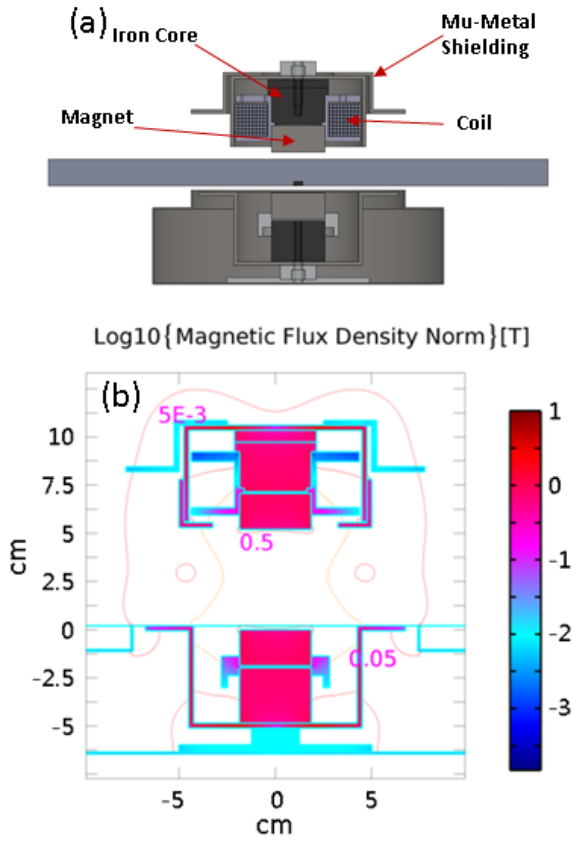

Fig. 2. (a) Cross-sectional diagram of the upper and lower assemblies. (b) Magnetic field strength distribution around the upper and lower assemblies. The model shows the effectiveness of the mu-metal shielding in reducing the magnetic field outside of the assemblies.

3. ACTUATING

3.1. Electromagnetic Coil

The electromagnet coil used in the experiment consists of a multi-turn coil. The coil is driven by an H-bridge circuit that is controlled by a pulse-width modulated signal. In the ideal case the lower assembly will be suspended such that the average current flowing through the coil is zero. However this is not always the case, and since the coil is placed in vacuum heat dissipation becomes a concern. In the original MSS, which used a NdFeB (neodymium) magnet, local heating by the coil may have lowered the magnetization of the permanent magnet, weakening the force between the upper and lower assembly. In the upgraded real MSS we will switch to SmCo (samarium−cobalt) magnets which have a Curie temperature of approximately 2.5 times that of NdFeB magnets.

3.2. Permanent Magnet

Understanding the magnetic field distribution and strength around the magnet assemblies is essential to ensure the field does not couple to some external magnetic material. Additionally, the field gradient along the axial direction determines the magnetic force between the magnets and thus the maximum load. The 2009 paper by Jabbour et al. [6] examined the magnetic field distribution of the original system. However, the finite element modeling (FEM) was not compared to real-world data and several changes have been made to the system, including the switch to SmCo magnets. A 2D cross-section of the current design is shown in Fig. 2a. The modeling of the field, Fig. 2b, is carried out using the commercial software COMSOL[1]. To facilitate an understanding of the modeling and to validate its usage we started with a simple system that could be checked against analytic solutions and simulations and then moved to the full system.

Cylinder Magnet

The core component of the magnetic suspension system is the cylindrical permanent magnet used to produce the dc magnetic field. The majority of the pulling force used in the suspension results from this field. In the current

[1]Certain commercial equipment, instruments, or materials are identified in this paper in order to specify the experimental procedure adequately. Such identification is not intended to imply recommendation or endorsement by the National Institute of Standards and Technology, nor is it intended to imply that the materials or equipment identified are necessarily the best available for the purpose.

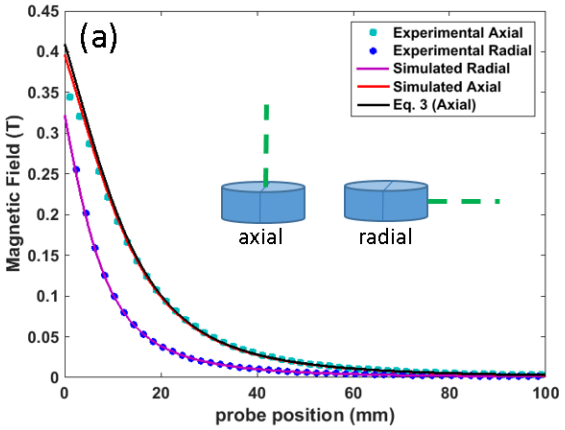

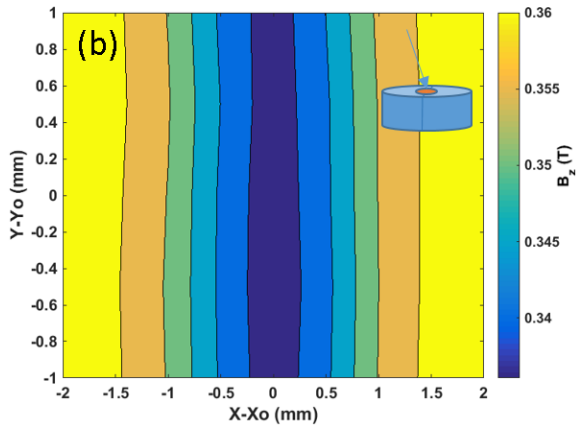

Fig. 3. (a) Magnetic field strength measured along the axial and radial direction. (b) Magnetic field strength measured radially about the center of the magnet, 1.05 mm off the surface. Here a lack of axial symmetry can be clearly identified.

design, the magnet has a height of 19 mm and a diameter of 38 mm. We focus here on a SmCo magnet with a residual flux density of $B_{res} = 1.16$ T.

A common approach to deriving an analytic expression, in the case of no current density, is to use a scalar magnetic potential:

$$\Psi = \int_V \frac{\rho_m(\vec{r})dr}{4\pi\mu_0|\vec{r} - \vec{r}'|}, \tag{1}$$

where $\rho_m(\vec{r})$ is the magnetic charge density and μ_0 is permeability of free space. The magnetic field can be determined by inserting Ψ into

$$\vec{H} = \vec{\nabla}\Psi \tag{2}$$

and using $B_z = \mu_0 H_z$. The resulting magnetic field strength is

$$B_z = \frac{B_{res}}{2}\left(\frac{z - d/2}{\sqrt{R^2 + (z - d/2)^2}} - \frac{z + d/2}{\sqrt{R^2 + (z + d/2)^2}}\right). \tag{3}$$

Here R and d are, respectively, the radius and height of the cylinder and z is the distance the field is measured from the center of the magnet.

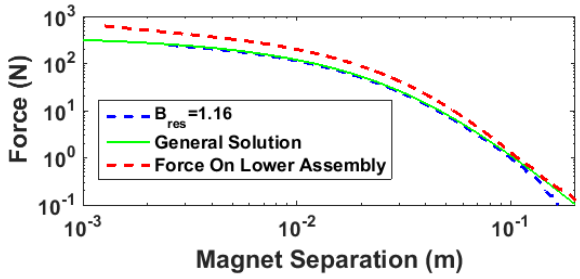

Fig. 4. Comparison of FEM calculation (blue dashed) for two cylindrical SmCo magnets to analytic expression (green line), (5), for the magnetic force. The red dashed line is the FEM calculation for the force on the entire lower assembly.

Using Ampere's law we carry out an FEM of the system to determine the field. To decrease computation time, we take advantage of the 2D axial symmetry of the model. Within the geometry we also add a small fillet to the corners of the magnets, while this does not impact the resultant field, it can have a substantial impact on the force calculation. The material property is chosen to be iron, however the relative magnetic permeability and residual flux density are set to those of SmCo, namely $\rho = 1.05$ and $B_{res} = 1.16$ T, respectively. This choice captures the essence of the important magnetic properties of the material.

A comparison of the results is shown in Fig. 3a, where strong agreement is seen except near the surface where the measured field decreases. The radial measurements in Fig. 3a, also show strong agreement. Finally, in Fig. 3b the field around the central axis at a fixed axial separation is measured. While for true axial symmetry a radial distribution would be expected, here, a clear breaking of this symmetry is found. This deviation is the same decrease seen in Fig. 3a, and results from a small residual magnetization pointing inward along the x-axis, toward the center that resulted from the manufacturing process. This unexpected result should not negatively impact performance, and may help dampen rotation of the lower magnet about its axial axis while suspended.

Magnetic Force

A closed-form solution for the force between two cylindrical magnets can be derived [7]. The general expression is

$$F_z = \frac{\partial E}{\partial z} = 2\pi\mu_0 M^2 R^3 \frac{\partial J_d}{\partial z}, \tag{4}$$

from which a general solution can be found:

$$F_z = -2\pi K_d R^2 \sum_{i,j=-1}^{1} i \cdot j \cdot A_{11}^0(\zeta + i\tau_1 + j\tau_2, 1, 1), \tag{5}$$

where $K_d = \mu_0 M^2/2$ and

$$A_{11}^0(\omega, 1, 1) = \frac{\omega}{\pi k_1}E(k_1^2) - \frac{(2 + 0.5\omega^2)k_1\omega}{2\pi}K(k_1^2) + \frac{1}{2}. \tag{6}$$

K and E are complete elliptic integrals of the first and second kind and $k_1^2 = 4/(4+\omega^2)$. As seen in Fig. 4 the general solution shows excellent agreement for separations up to 10 cm; beyond this distance the FEM breaks down. An expression for the force acting on the entire lower assembly is more difficult to derive, so the FEM is necessary to determine the force.

4. SENSING

4.1. Hall probe

A Hall probe is placed between the two magnet assemblies to monitor the magnetic field. The field indicates the relative separation of the two magnets and thus provides a good signal for the servo to stabilize. As part of the effort to improve the overall system we will move to a Hall probe with a lower noise floor. As is often the case during such a testing period we have also identified limitations in the current A/D conversion of the signal. We are working to implement fixes that will lead to a decrease in the minimum resolution of the measured signal.

4.2. Interferometer

Given the measurements made of the Hall probe signal and the magnetic field gradient computed based on simulation, a lower limit on the position resolution and ultimate stability of the suspended mass can be determined. To further decrease this value, efforts have been made to design and implement an interferometer to detect fine motion of the suspended assembly.

The simplified approach, as shown in Fig. 1, involves configuring the interferometer such that its measurement arm is directly below the suspended assembly. In this way, vertical motion can be detected. The interferometry is based on a heterodyne measurement. Two orthogonally polarized beams of light, shifted in frequency by 2.8 MHz, are injected into a fiber and passed into the lower chamber. The beams are then sent through a polarizing beam splitter. One polarization becomes the reference arm of the interferometer while the other is the measurement arm that is bounced off the suspended assembly. The beams are recombined and sent back through the fiber where they are passed through a polarizer set at 45° and then measured using a photo-detector. The electrical response is then demodulated at the unperturbed frequency difference. The movement of the hanging assembly Doppler shifts the measurement beam, which leads to a frequency difference. This difference can be converted to determine both the velocity and the displacement of the suspended lower magnetic assembly.

5. CONTROL

To control and stabilize the suspended mass, feedback is used. In the previous generation the MSS feedback was carried out by a PID loop that was implemented and run directly from a desktop computer. Typical computer latency led to jitter in the feedback loop rate, this in turn led to instabilities in the suspension of the mass. We have since moved the entire feedback system to a field programmable gate array (FPGA). The FPGA approach provides a deterministic loop rate from which to implement the feedback. We currently run at a rate of 100 kHz, an order of magnitude faster than the average loop rate we could previously obtain. Additionally, because of the ease of altering code on the FPGA, as opposed to a pure analog approach, the use of multiple control signals (Hall sensor, interferometric velocity and displacement) is simplified. Of course, we have to confront resolution issues resulting from the limited number of bits available for digitization.

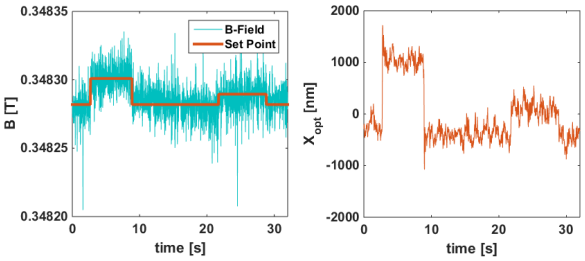

Fig. 5. Control of suspended mass by varying set point. Using interferometer coupled with the Hall sensor vertical displacement less than 500 nm can be actuated and detected.

Using the test MSS we have implemented the new FPGA code for system control. This in conjunction with a 24-bit ADC and the newly added interferometric signal has provided a high level of control within the system. In Fig. 5, we show changes to the measured magnetic field as well as the optically measured displacement of the suspended mass pan, resulting from small changes to the set point. Within the level of stability currently achieved with the test MSS we can clearly see sub-micron motion. At this time the mass stability is below the resolution (1 mg) of the comparator used in the test MSS. As such, no measurable change in mass is seen during the controlled displacements shown in Fig. 5.

6. CONCLUSIONS

NIST is actively working to develop a mise-en-pratique, a set of instructions for the definition of a unit that ensures it can be realized at the highest level of precision, for the redefinition of the kilogram. A critical component of this is the mass comparison of a mass standard in vacuum to a test mass in air. To that end, recent efforts have been focused on the magnetic suspension system. The system is currently being re-assembled in a newly renovated laboratory. Building on our experiences from the previous system and incorporating results from the tests and improvements described within this paper should provide a system that meets the demands of the mass community, i.e. mass comparison measurements with a standard uncertainty for 1 kg of less than 20×10^{-9} kg.

REFERENCES

[1] I. M. Mills, P. J. Mohr, T. J. Quinn, B. N. Taylor, and E. R. Williams, "Redefinition of the kilogram: a decision whose time has come," *Metrologia*, vol. 42, no. 2, p. 71, 2005.

[2] G. Girard, "The third periodic verification of national prototypes of the kilogram (1988-1992)," *Metrologia*, vol. 31, no. 4, p. 317, 1994.

[3] A. Picard and H. Fang, "Methods to determine water vapour sorption on mass standards," *Metrologia*, vol. 41, no. 4, p. 333, 2004.

[4] F. T. Holmes, "Axial magnetic suspensions," *Review of Scientific Instruments*, vol. 8, no. 11, pp. 444–447, 1937.

[5] S. Schlamminger, D. Haddad, F. Seifert, L. S. Chao, D. B. Newell, R. Liu, R. L. Steiner, and J. R. Pratt, "Determination of the planck constant using a watt balance with a superconducting magnet system at the national institute of standards and technology," *Metrologia*, vol. 51, no. 2, p. S15, 2014.

[6] Z. J. Jabbour, P. Abbott, E. Williams, R. Liu, and V. Lee, "Linking air and vacuum mass measurement by magnetic levitation," *Metrologia*, vol. 46, no. 3, p. 339, 2009.

[7] D. Vokoun, M. Beleggia, L. Heller, and P. ittner, "Magnetostatic interactions and forces between cylindrical permanent magnets," *Journal of Magnetism and Magnetic Materials*, vol. 321, no. 22, pp. 3758 – 3763, 2009.